On Part Load Recirculation of Pumps and Fans – a Generic Study

Dennis Stapp, Peter F. Pelz, Jan Martin Loens
Chair of Fluid System Technologies, Technische Universität Darmstadt, Germany

Email: sekretariat@fst.tu-darmstadt.de

Abstract. At part load in turbo machinery, there is a boundary layer separation resulting in a large vortex structure called part load recirculation. Up to now the influence of Reynolds number, relative roughness and degree of turbulence on this important stability limit of machines is not sufficiently understood. To shed some light onto these phenomena, in this work the simplest "machine" is considered by numerical and experimental studies. The apparatus we examine is a circular pipe at rest followed by a rotating co-axial pipe segment. By doing so, we have a generic test case which serves to study the critical flow number, defined by the onset of the separation and formation of a ring vortex.

1. Introduction

Turbo machines often operate below capacity (flow number φ), instead of their design point, to fulfill varying utilization requirements. When the flow number falls below a critical limit, the boundary layer in the impeller separates, forming a part load recirculation. This process limits the characteristic diagram for economic and reliable operation.

The phenomenon of part load circulation occurs even in the most abstract form of machine, the transition from a pipe at rest to a rotating, coaxial pipe. The present paper shows numerical and experimental results on the influence of the Reynolds number, the gap between both pipes and the surface roughness on the critical flow number φ_c using the following generic model shown in Fig. 1.

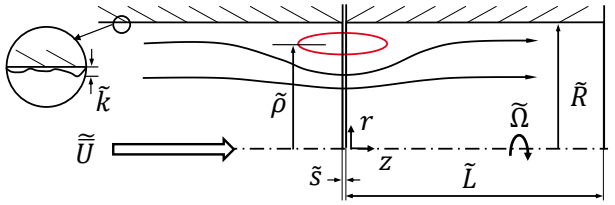

Fig. 1: Generic model of the part load recirculation. Dimensional physical quantities are signed with tilde.

As in a turbo machine the boundary layer separates and recirculates below a critical average flow $\tilde{\bar{U}}_c$ respectively below a critical flow number $\varphi_c := \tilde{\bar{U}}_c/(\tilde{\Omega}\tilde{R})$ from the rotating wall with a circular frequency $\tilde{\Omega}$ and radius $\tilde{R}$. In case of $\varphi < \varphi_c$ a coaxial vortex ring forms at the inlet of the rotating pipe, with a core radius $\tilde{\rho} = \tilde{\rho}(\tilde{\Omega}, \tilde{R}, \tilde{\bar{U}}, \tilde{k}, \tilde{s}, \tilde{L}, \nu \dots)$ The relevant parameters are: roughness $\tilde{k}$, length of the rotating pipe $\tilde{L}$, kinematic viscosity ν and gap width $\tilde{s}$. Is the pipe radius chosen as characteristic length and the rotational velocity of the pipe is chosen as characteristic speed, a dimensional analysis shows the dependency $\rho = \rho(Re, \varphi, k, s, L)$ with the Reynolds number $Re = 4\tilde{\Omega}\tilde{R}^2/\nu$. The dimensionless average flow velocity is defined as $\bar{U} := \varphi = \tilde{\bar{U}}/(\tilde{\Omega}\tilde{R})$, the relative roughness as $k = \tilde{k}/\tilde{R}$, the gap width as $s = \tilde{s}/\tilde{R}$ and the length of the rotating pipe as $L = \tilde{L}/\tilde{R}$.

The generic model is well described for separated laminar flow [1], [3], for attached turbulent flow, and turbulent flow in the fully developed region downstream the inlet [4], [5], [6]. For laminar flow it is known that the critical flow number increases with increasing Reynolds number $\varphi_c \sim Re$ for small Reynolds number [2], [7]. The present work describes the flow separation at the inlet area regarding technical relevant high Reynolds numbers.

2. Numerical results

In the ideal case, the transition between the pipe at rest and the rotating pipe is discontinuous, the gap width $s = 0$. The flow is incompressible and stationary.

2.1. Numerical setup

The simulated mesh is axis symmetrical with resolved boundary layer in order to reach $y_+ = \Delta y/\delta_v < 1$, with the viscous length $\delta_v := \nu/u_*$. The mesh consists of $1.6 \cdot 10^5$ nodes and is divided into three sections as shown in Fig. 3. Section I represents the static pipe, its left boundary is defined as a velocity inlet with the mean velocity $\overline{U} = 1$. The upper boundary is defined as a static wall with varying roughness. Section II represents the rotating pipe; its upper wall is defined as a rotating wall with rotational frequency $\Omega := 1/\varphi$ and the same roughness as the static pipe. Section III represents a free stream area with a pressure outlet $p = 0$. The Reynolds number is varied by the kinematic viscosity of the fluid $\nu := \varphi^{-1} Re^{-1}$. For modeling turbulence, the Transition Shear Stress Model (Transition SST) without wall function is used. This is a four equations model based on the two $k - \omega$ SST transport equations with two additions: one additional equation for the intermittency and one for the onset of transition.

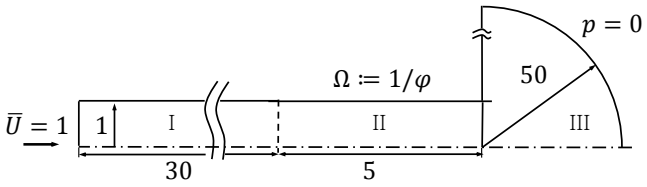

Fig. 3: Mesh and boundary conditions.

2.2. Separation phenomena and criteria

The recirculation is identified by its local maximum of the stream function on the coordinate of the vortex core. For a large flow number and due to attached flow, the maximum of the stream function is located on the rotating wall $\rho = 1$. Fig. 4 shows the radial vortex core coordinate depending on the flow number. The expansion of the vortex core to $\rho = 0.99$ is defined as separation criterion and $\varphi_c = \varphi(\rho = 0.99)$ as critical flow number. Because it is nearly impossible to find an accurate state of $\rho = 0.99$, the interpolation between the nearest simulation points is shown in Fig. 6 as an error bar. Fig. 4 also shows the streamlines in two variations: once for $\varphi > \varphi_c$ and once for $\varphi < \varphi_c$. In the separated case $\varphi < \varphi_c$ there is a negative axial velocity near the wall indicating a backflow.

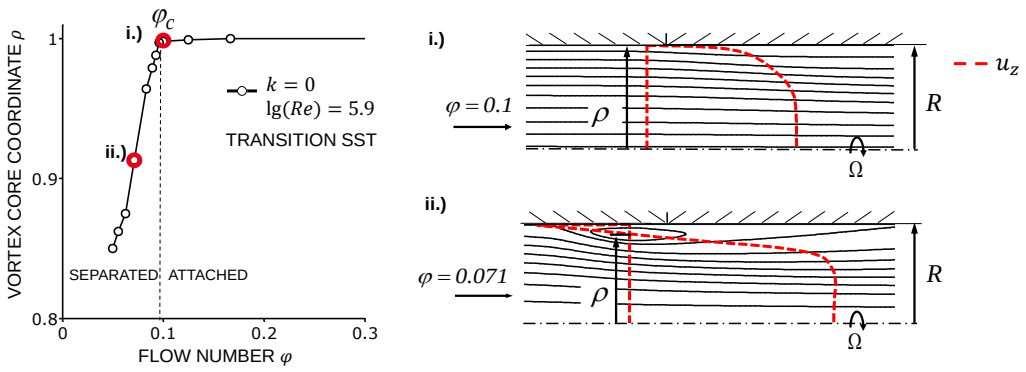

Fig. 4: Left, Vortex core coordinate vs. flow number for an ideal case $s = 0$. Right, streamlines and axial velocity profile u_z for i.) separated and ii.) attached flow.

2.3. Influence of Reynolds number and roughness

The Reynolds number affects the onset of the flow separation as well as the radial trajectory of the vortex core depending on the flow number. In the considered range, the critical flow number decreases with increasing Reynolds number. For higher Reynolds numbers, the expansion of the separation becomes more abrupt as shown in Fig. 5. The simulation results in Fig. 6 show that the critical flow number increases with increasing roughness. There is a lower limit depending on the Reynolds number that limits the effect of roughness, the hydraulic smooth case. The hydraulic smooth roughness decreases with increasing Reynolds number.

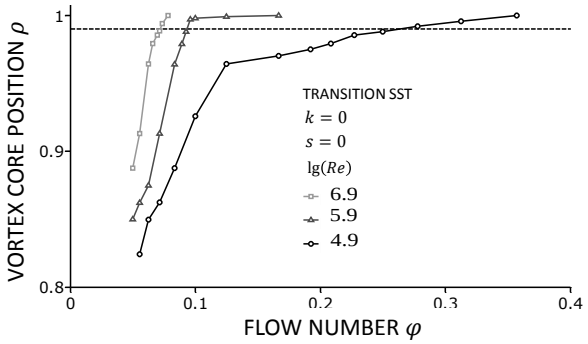

Fig. 5: Vortex core trajectory vs. flow number.

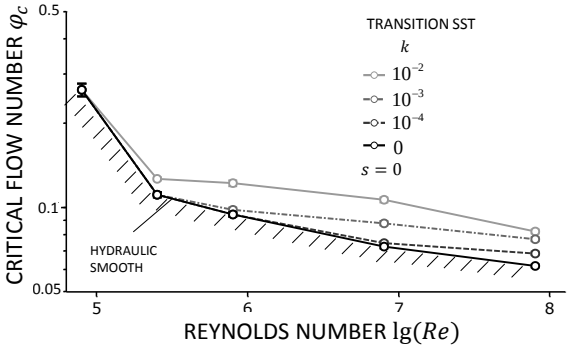

Fig. 6: Influence of relative roughness and Reynolds number on the critical flow number.

2.4. Influence of discretisation and turbulence model

The mesh study contains a fine mesh with four times more cells and a coarse mesh with four times less cells than the used standard mesh. The study shows that the simulation result is only influenced negligibly by varying mesh discretisation on the critical flow number with an error in the scale of 2%. For small Reynolds numbers it is less than the interpolation error.

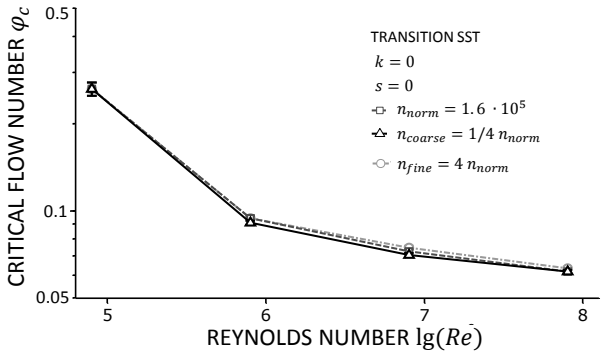

Fig. 7: Mesh studies, influence of discretization.

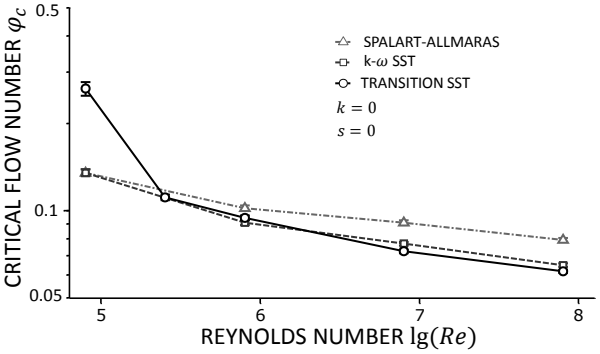

Fig. 8: Turbulence model studies.

For the turbulence model study two further turbulence models are used. The Spalart-Allmaras is a so called one-equation model that has one modelled transport equation for the kinematic eddy (turbulent) viscosity. The k-ω SST model is a two-equation model with a blending function for the k-ω formulation at the near wall region flow and the k-ϵ formulation for the far field.

The results in Fig. 8 show a good accordance of the Transition SST and the k-ω SST model for larger Reynolds numbers. For $\lg(Re) < 5.5$ the Transition SST model predicts an increase of the critical flow number that is not shown by the k-ω SST model. The prediction of the Spalart-Allmaras model intersects with the prediction of the Transition SST model. Like the k-ω SST it shows no significant rise of the critical flow number for small Reynolds numbers.

2.5. Pipe with gap width $s > 0$

Concerning a real machine, the minimum gap width between the rotating and the static pipe is limited by the bearing stiffness and the accuracy of manufacturing. The gap disrupts the boundary layer and causes a secondary flow in the gap, which interacts with the mainstream and induces a pre-rotation.

As section IV of the mesh, there is a gap between the static and the rotating pipe with a width of $s = 0.004$ and a depth of 0.2. The right boundary of the gap section is part of the rotating wall and it is simulated as rotating wall with the same rotating frequency. The upper and left boundaries of the gap are static walls. Fig. 9 visualizes the streamlines for the simulation of separated flow. Remarkable is that the recirculating flow transports swirling fluid upstream over the gap into the static pipe.

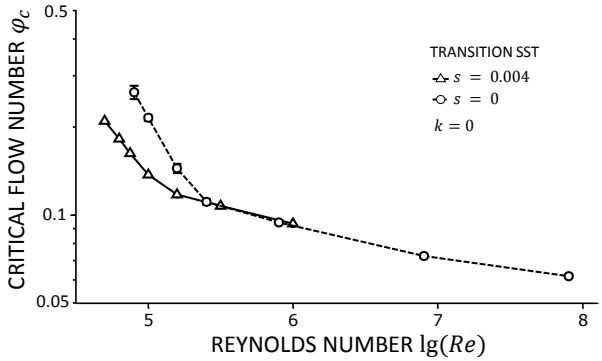

Fig. 8: Influence of the gap on the critical flow number.

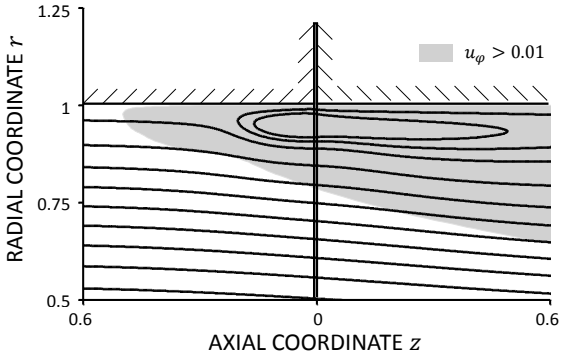

Fig. 9: Streamlines and circumferential velocity $s = 0.004,\ k = 0,\ lg(Re) = 5, \varphi = 0.1$ Transition SST.

The progression of the critical flow number in the logarithm diagram on Fig. 8 is described by two tangents and their intersection at the *critical Reynolds number* Re_*. The critical flow number follows in the considered region the exponential law $\varphi_c \sim Re^{-n}$ with an exponent $n = n_u$ for the under critical area $Re < Re_*$ and $n = n_o$ for $Re > Re_*$ with $n_u > n_o$. The existence of the gap reduces the value of the critical Reynolds number. In the configuration without a gap the critical Reynolds number is predicted to $\lg(Re_*) \approx 5.2$, in the configuration with a gap it is predicted to $\lg(Re_*) \approx 5$. For $\lg(Re) > 5.5$ the gap has only small influence on the predicted critical flow number.

3. Experimental results

For the experimental investigation a free stream channel with a radius of $\tilde{R} = 0.025\ m$ and air as fluid is used. The Mach number of the flow is smaller than 0.1, therefore the flow can be considered as incompressible. To measure the flow field, a 1D Laser Doppler Anemometry (LDA) system with an aerosol of silicon oil as tracer particles is used. The measured velocities are averaged over 40 seconds.

3.1.1. *Experimental setup*

The air flow for the experiment is provided by a radial fan. To reduce pulsing of the flow, the fan is separated from the channel by a large plenum chamber and a flow resistance. At the inlet to the channel, an aerosol of silicon oil as tracer particle is added to the air and it is directed into an integrated conditioning chamber with a flow rectifier and three turbulence screens. It follows a pipe of $60\ \tilde{R}$ length and passes an obstacle. Then the flow is directed through a geometrical high precision pipe with the length of $15\ \tilde{R}$ into the rotational unit shown in Fig. 10. The rotating pipe has a length of $5\ \tilde{R}$ and a relative roughness of $k < 10^{-4}$, because the limiting case of a semi-infinite pipe is reached for $L > 5$, as a result of numerical analysis. To avoid leakage through the gap, the spindle ball bearings are sealed. The probe for the 1D LDA measurement has a focus of 315 mm and is located downstream of the outlet in an angle of 12 degrees. It is adjusted to measure only the swirl component of the flow.

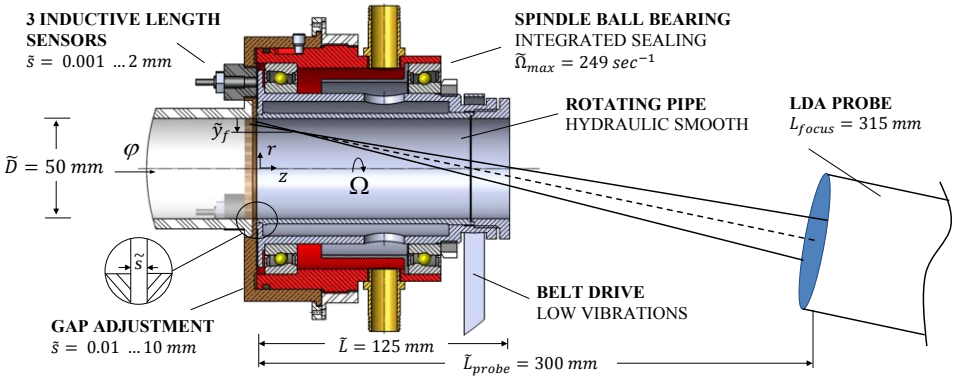

Fig. 10: Geometry and characteristics of the rotation unit and the measurement system

3.1.2. LDA measurement and separation criteria

With LDA, the development of the swirl velocity in a circumferential boundary layer is measured. In comprehension to the numerical results a swirl component in the static pipe is an indication for a flow separation with a backflow that transports the swirl velocity upstream. For the indication of the critical flow number the measurement volume is positioned at the entry of the rotating pipe at $z = 0$ and a wall distance $y_f = \tilde{y}_f/\tilde{R}$ of 0.024. Fig 11 shows the measured circumferential velocity over varying flow number for different wall distances of the measurement volume (left) and the circumferential boundary layer for particular flow number (right).

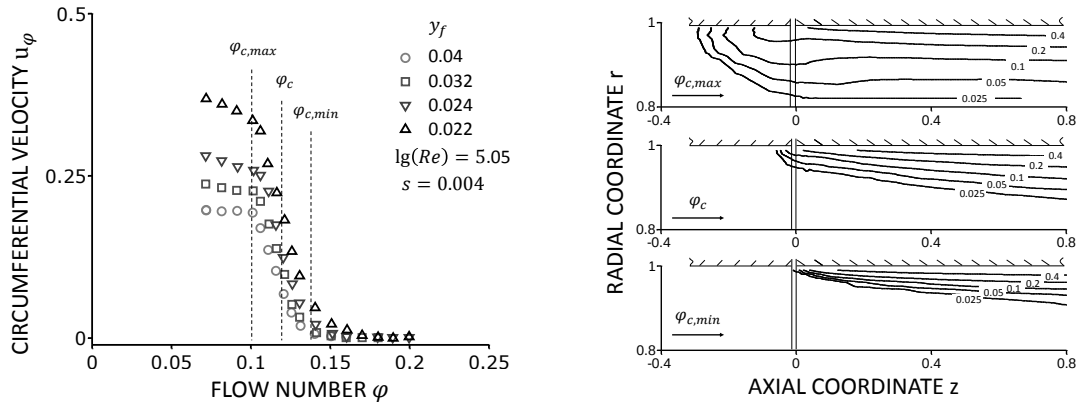

Fig. 11: Left, measured circumferential velocity varying radial positions of the measurement volume and flow number. Right, swirl velocity distribution for the identified maximal, minimal and the chosen critical flow number.

While the flow is attached, the swirl component at the measurement position is small and only affected by pre-rotation from the mixing zone in the gap. The circumferential boundary layer of the rotating pipe during attached flow is thin and does not reach the measurement volume. Reducing the flow number below a certain limit leads to an abrupt growing of the circumferential boundary layer thickness and therefore to an abrupt rise of the measured swirl component in Fig. 11. Remarkable for the expansion is that the effect can be measured on different wall distances at the same flow number. A reduction of the flow number below the rising edge affects a moderate increase or even a small decrease of measured swirl velocity. The critical flow number φ_c is defined with regards to the intersection point $\varphi_{c,max}$ of a tangent to the upper level and the rising edge. The point where the rising edge reaches $u_\varphi(\varphi_{c,max})/2$ marks the critical flow number. The separation of the flow is assumed as a span between $\varphi_{c,min}$ and $\varphi_{c,max}$.

3.1.3. Separation for different Reynolds numbers

The Reynolds number is varied from $\lg(Re) = 4.75$ to $\lg(Re) = 5.23$. In all investigated conditions the axial Reynolds number $Re_{ax} = \bar{U}R/\nu$ >3500 is applied. The results of the LDA measurement in Fig. 12 show that an increasing Reynolds number causes a decrease of the critical flow number. As in

the numerical investigation, the progression of the critical flow number in the logarithm diagram in Fig. 13 can be approximated by two tangents which intersect at the critical Reynolds number. The critical flow number again follows $\varphi_c \sim Re^{-n}$. with an exponent n that decreases for $lg(Re) > lg(Re_*) \approx 5$ and converges to a constant tangent in the logarithm diagram.

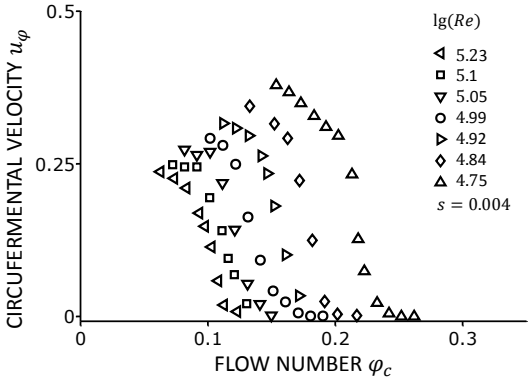

Fig. 12: LDA measurement of swirl velocity vs. Reynolds number and flow number, $y_f = 0.024$.

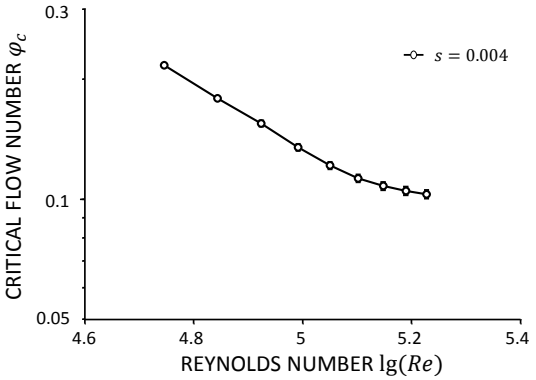

Fig. 13: Measured critical flow number vs. Reynolds number.

4. Conclusion

The present work extends the knowledge concerning the onset of flow separation in a rotating pipe to high Reynolds numbers, which is of particular relevance for turbo-machines. The achieved experimental data are in good accordance with the numerical results and indicate that the critical flow number decreases with an increasing Reynolds number. Independent from the criterion used for separation detection, the critical flow number can be determined by the aid of two tangents, described by the exponential law $\varphi_c \sim Re^{-n}$, leading to a constant exponent n for each tangent. The intersection point of these tangents represents the critical Reynolds number Re_*. For $Re > Re_*$ the exponent n is reduced. The numerical results show, that the value of Re_* depends on the existence of a gap between the pipe at rest and the rotating pipe.

Further research work will be focused on investigation of the axial and the circumferential boundary layer in order to analyze their independency. The long-term objective of the current scientific work is to establish an appropriate physical model describing the development of turbulent boundary layer and separation due to a swirl induced positive pressure gradient on the rotating wall. Such a model could be used to predict the onset of part load recirculation in real turbo-machines.

5. References

[1] A. White, "Flow of a fluid in an axially rotating pipe," *Journal of Mechanical Engineering Science,* 1964.

[2] S. Imao, Q. Zhang and Y. Yamada, "The laminar flow in the developing region of a rotating pipe," *JSME International journal,* vol. 32, pp. 317 - 323, 1989.

[3] L. Facciolo, N. Tillmark, A. Talamelli and P. H. Alfredsson, "A study of swirling turbulent pipe and jet flows," *Physics of fluids,* vol. 19, 2007.

[4] K. Nishibori, K. Kikuyama and M. Murakami, "Laminarization of turbulent flow in the inlet region of an axially rotating pipe," *JSME International journal,* pp. 255 - 262, 1987.

[5] M. Oberlack, "Similarity in non-rotating and rotating turbulent pipe flows," *Journal of Fluid Mechanics,* vol. 379, pp. 1-22, 1999.

[6] Z. Lavan, "Separation and Flow Reversal in Swirling Flows in Circular Ducts," *Physics of Fluids,* vol. 12, no. 9, pp. 1747-1757, 1969.

[7] C. Crane and D. Burley, "Numerical studies of laminar flow in ducts and pipes," *Journal of Computational and Applied Mathematics,* vol. 2, no. 2, pp. 95--111, 1976.